International Journal of Academic Engineering Research (IJAER)
ISSN: 2643-9085
Vol. 5 Issue 3, March - 2021, Pages: 8-19

Constitutive Relationship of Fusion Zone In The Spot Welds of Advance High $_T$ Strength Steels

Jurabek Abdiyev[1], Elyor G'aybulloyev[2], Sherzod Yarashev[2*], Begzod Erkinov[2]

[1]Physical-technical Institute of NPO "Physics – Sun" of Uzbekistan Academy of Sciences Uzbekistan, Tashkent, Chingiz Aitmatov street 2B.

[2]Tashkent University of Information Technologies named after Muhammad al-Khwarizmi, Uzbekistan, Tashkent, Amir Temur street 108.

Corresponding author: sherzodyarashev1997@gmail.com (Sh. Yarashev)

Abstract *– Constitutive relationship of fusion zone is essential for a practical numerical model to analyze the fracture behavior of resistance spot welded advance high strength steels. In this paper, the constitutive relationship was directly measured by developing a simple but effective experimental setup with the new small tensile specimen that could be available in typical universal tensile machines. This new specimen was used to characterize the key properties of fusion zones in the spot welds of DP590 steels, Q&P980 steels and 22MnB5 steels. Compared to the ultimate tensile strength in the fusion zone of DP590 steels and 22MnB5 steels with the value of 1100 MPa, the strength was up to 1700 MPa in the fusion zone of Q&P980 steels due to the formation of retained austenite. Strain distribution results indicate that the heterogenous microstructure with smaller grain misorientation in the fusion zone of Q&P980 steels leads to the larger fracture strain in a comparison to other fusion zones. These results revealed that the fusion zone of Q&P980 steels exhibited a superior strength and ductility compared to that of DP590 steels and 22MnB5 steels.*

Keywords – Fusion zone, Constitutive relationship, Small tensile specimen

1. INTRODUCTION

Resistance spot welding (RSW) was one of the primary methods in automotive industry for joining advance high strength steels (AHSSs), due to the advantages of low cost, high efficiency and easy automation [1–3]. The mechanical performance in the spot welds of AHSSs, especially in terms of strength and failure mode, was closely related to the material properties of fusion zone [4–6]. To access failure behavior, such as by finite-element methods, researches required an accurate description of the constitutive relationship in the fusion zone [7–9]. Due to the small region and heterogenous microstructure in the fusion zone, the constitutive relationship of fusion zone was still the issue for numerical model developers to predict failure mechanism of spot welds.

Hardness extrapolation method had been used to characterize the constitutive relationship of fusion zone. The method deducted the constitutive relationship of fusion zone based on the hardness ratio between different microstructures and the measured constitutive relationship of base metal or composition phase [10]. Wang [11] obtained the constitutive relationship of fusion zone by assuming that there was a linear relation between the stress-strain curves of base metal, aiming to develop numerical model to predict the failure behavior in the spot welds of HSLA 350. Eller [12] focused on the phase difference in fusion zone and established the constitutive relationship of fusion zone based on the stress-strain curves of different microstructures in the fusion zone. This method used material hardness as driving parameter for constitutive model. However, the hardness distribution in the fusion zone could not comparatively describe the strength and ductility in the zone, resulting in plausible inaccurate results of constitutive relationship.

Recently, the researches sought an experimental method that could directly characterize the constitutive relationship of fusion zone in spot welds. Due to the small size of fusion zone, the characterization is more difficult than the base metal with dimension specified in ISO standard. The key issue for the measurement of constitutive relationship in the fusion zone is the experimental setup, including the specimen preparation and the experimental systems. One of the promising methods was extracting sub size tensile bar from spot welds to measure the constitutive relationship of fusion zone using extensometer. The method has been applied to determine the constitutive relationship of fusion zone in aluminum alloy spot welds [13], mechanical properties of resistance spot welded AHSSs [14] and dynamic stress-strain curves of TRIP690 steel joint [15]. This method provided an approach for measuring the stress-strain curves in the fusion zone. However, the parallel region of dog-bone specimen contains fusion zone, heat-affected zone and/or base metal. The effect of heat-affected zone is hard to eliminate in the method.

Another promising method is the directly measurement of constitutive relationship of fusion zone. To obtain the strain distribution, compared to the conventional strain measurement technique, such as extensometer, DIC (Digital image correlation) method could be an effective way to in-situ measure the plastic deformation of extremely small area and calculate the strain evolution. Chen [16,17] found that DIC technique could be suitable to for in-situ measurement of stain evolution of strain near the fusion zone during the arc welding process. Wei [18] designed a miniature tensile bar totally extracted from fusion zone to measure the constitutive relationship of fusion zone in dual-phase steel with assistance of DIC device. Park [19] used the miniature tensile bar extracted from the resistance spot-welded DP980 joint to access the true stress-strain curve of fusion zone at various

strain rates by DIC technique. However, the miniature tensile bar with small size of 2 mm*2 mm has several disadvantages for strain measurement. First of all, due to the extremely small size of specimen, the miniature tensile bar posed challenges for the manufacturing process because the un-avoidable bending deformation. Secondly, to conduct tensile tests for the miniature tensile bar, tensile fixture should be tailored according to the specimen geometry, leading to the restriction of application.

Unlike the previous miniature specimen with dimensions of about 2 mm*2 mm, this paper proposed a new small tensile specimen with geometry of 85 mm*17 mm. The new specimen was thinned in the fusion zone with dimension of 3 mm*3 mm so that the plastic deformation and fracture were occurred in the fusion zone because the non-uniform deformation. It is easy to install the specimen to conduct the tensile tests using typical universal material testing machines. Hence, the new small tensile specimen could be used to directly measure the constitutive relationship of fusion zone using typical universal material testing machines. In this paper, constitutive relationship of fusion zone was extracted from small tensile specimen taken from resistance spot-welded Q&P980 steels and systematically compared with that of DP590 steels and 22MnB5 steels.

2. EXPERIMENTAL PROCEDURE.

2.1. MATERIALS

The investigated materials are Q&P980 steels, DP590 steels and 22MnB5 steels with thickness of 2 mm. Fig. 1 describes the micro-structure in the base metal of three investigated steels. The micro-structure of Q&P980 steels, shown in Fig. 1(a), consists of a ferrite matrix with retained austenite and finely dispersed martensite. The Q& P980 steels were produced by a quenching and partitioning process. The partitioning process reduces the carbon in martensite leading to the crystal parameters of BCT structure closer to the cubic ferrite, which attribution to the formation of softer martensite with dispersed distribution. The microstructure shown in Fig. 1(b) describes that the microstructure of DP590 steels is composited of a ferrite matrix with dispersed martensite at the grain boundaries. 22MnB5 steels (as illu-strated in Fig. 1(c)), obtained by a hot stamping heat treatment process, consists of fully martensite with hardened state. Besides, the chemical composition and mechanical properties of the three steels are shown in Table 1.

2.2. SPECIMEN PREPARATION

The steel sheet with dimension of 150 × 50 mm plates were used to produce resistance spot welds, designed for preparation of small tensile specimen. The welding parameters selected were according to AWS D8.9M:2012. The squeezing time, welding time and holding time was 1000 ms, 580 ms and 200 ms, respectively. Welding current was selected as 13 kA with an applied electrode force of 6.0 kN.

Small tensile specimens were extracted by electrical discharge machine (EDM) from the spot welds with feed rate of 5 mm/min, aiming to eliminate the effect of cutting process. As shown in Fig. 2(a), the location of small tensile specimen was in the center of spot welds, indicating the maximum use in the fusion zone. The specimen geometry is illustrated in Fig. 2(b). For the parallel region of dog-bone specimen, the length and width were selected as 3 mm to maintain the sufficient stiffness of specimen [20]. The gripped area is about 40 mm in the specimen and the specimen could be tested in the universal material testing machine without tailored fixture.

2.3. DIGITAL IMAGE CORRELATION

Fig. 3 described the experimental setup to measure the constitutive relationship of fusion zone, including equipped tensile machine and DIC system. The tensile tests were conducted by SUNS 5000 universal ma-terial testing machine with a tensile speed of 0.05 mm/s. DIC system contains an industrial camera of MV-3000UC and a complementary metal-oxide semiconductor (CMOS) with 2048 × 1536 pixels. The bracket was used to improve the image resolution by adjusting the distance between industrial focus and the specimen. Before the tensile tests, the specimens were sprayed with a combination of white paint and black paint before tensile tests to create image contrast for subsequently image correlation. Five replicates were conducted for each test.

The captured images were processed by Matlab codes to obtain the strain distribution and constitutive relationship of fusion zone. First, obtain the initial picture captured by DIC device. Then, the reference points were first generated in the selected grid of parallel region. The selected region was analyzed with a size grid of 10 × 10 pixels (32 × 32 μm) for deformation analysis. Several hundred images were captured for each tensile test and subsequently analyzed to infer the corresponding displacement and strain mapping. The program was used to analyze the displacement of reference points during the evolution of digital images and the strain was calculated by the modified Matlab codes for large displacement tracking [21,22].

The constitutive relationship was perceived based on the afore-mentioned experimental setup and data processing method. The strain was extracted from parallel region with the assistance of DIC data processing method. The stress was calculated by tensile force obtained from tensile machine. Strain and stress were matched based on the same frequency of data output in tensile machine

and picture capturing of industry camera. The DIC camera was about 40 cm separate from the small tensile specimen and the in-plane strain at the maximum depth was of about 1.0 mm. Thus, the in-plane strain error induced by out-of-

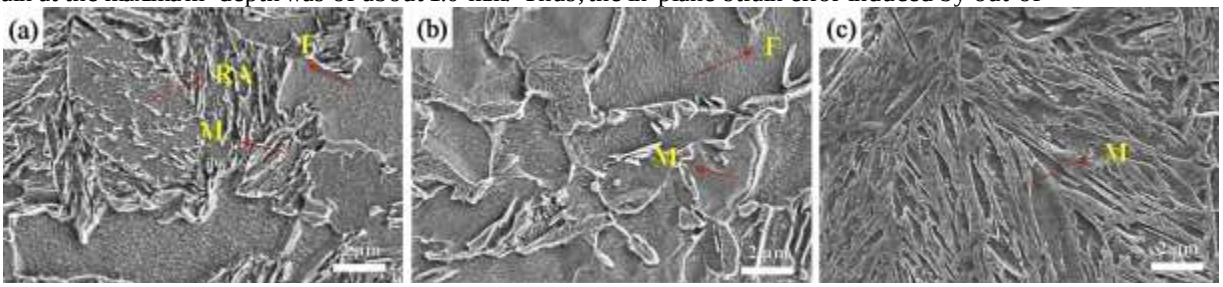

Fig. 1. Microstructure characterization of base metal in (a) Q&P980 steels, (b) DP590 steels and (c) 22MnB5 steels. F, M, RA is the abbreviation of ferrite, martensite and retained austenite, respectively.

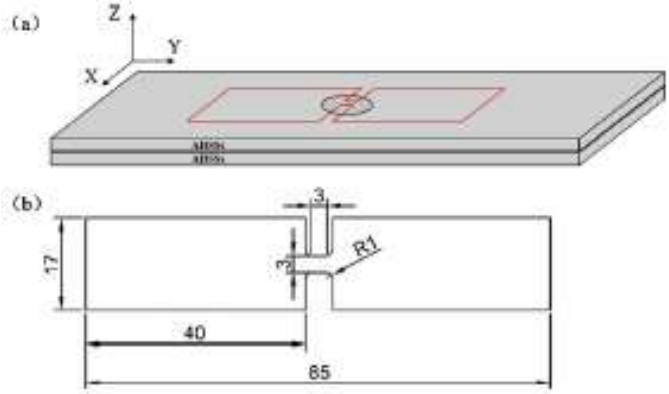

Fig. 2. Small tensile specimen preparation: (a) Location of specimen in the spot welds; (b) Geometry of small tensile specimen.

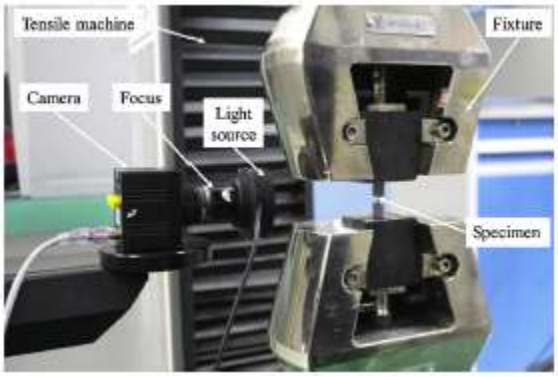

Fig. 3. Experimental setup coupling with tensile machine and DIC device for measuring the constitutive relationship of fusion zone using designed small tensile specimen.

plane displacement was of about 1%. Thus, the out-of-plane error could be neglected [23].

2.4. TESTING METHOD

Cross-section tests of spot welds was mechanically polished and the etched with a solution of 4% nital to reveal the nugget pro file. The SEM tests are conducted by a Zeiss Ultra Plus field Emission Scanning electron microscope with an electric voltage of 20 kV and a working distance of 8 mm to investigate the microstructure in the spot welds. The EBSD tests were conducted by TESCAN MIRA3 with an operating voltage of 20 kV and a step size of 0.05 μm.

3. RESULTS.

3.1. MICROSTRUCTURE

Constitutive relationship and fracture behavior of the fusion zones are significantly affected by the microstructural characteristics. Fig. 4 depicts the typical microstructure of fusion zone in spot welds of Q& P980 steels, DP590 steels and 22MnB5 steels.

Columnar structure is observed in the three fusion zones due to the rapid cooling rate during the welding process. The cooling rates are about 2000 K/s resulting in martensite transformation according to the continuous cooling trans-formation curves [8]. However, the microstructure morphology varies for different steels. In the case of fusion zone in Q&P980 steels (as shown in Fig. 4(a)), the crystallographic features are lath martensite and retained austenite in the zone. On the condition of DP590 steels described in Fig. 4(b), fusion zone solidifies with needle-like martensite. Besides, block martensite forms in the fusion zone of 22MnB5 steels as revealed in Fig. 4(c).

Fig. 4(d)–(f) displays the results of phase distribution in the three fusion zones of resistance spot welded Q&P980 steels, DP590 steels and 22MnB5 steels. As depicted, both martensite and retained austenite were observed in the fusion zone of Q&P980 steels. By contrast, only martensite was formed in the fusion zones of DP590 steels and 22MnB5 steels. Retained austenite in the fusion zone of Q&P980 steels could accommodate the dynamic strain and have effect on the mechanical properties of fusion zone. Thus, different phase distributions in the three fusion zones are supposed to results in variation of mechanical properties.

This microstructure difference could be largely attributed to the variation of microstructures in the base metal. Rich-carbon austenite in the Q&P980 steels impedes the austenite to martensite transformation during the welding process, resulting in the sufficient time for grain growth of martensite and the formation of retained austenite in the fusion zone. In the case of fusion zone in spot welds of DP590 steels, high Mn content attributes to the martensite formation during RSW process, which leads to solidify with a needle-like structure of fusion zone. The final microstructure of fusion zone in 22MnB5 steels is fully martensite, and block structure is observed in the zone caused by the high carbon content in the microstructure with fully martensite of base metal, which will impedes the nucleation during the welding process [24].

Fig. 5 illustrates the grain characterization results in the fusion zone of the three investigated steels. As shown in Fig. 5(a)–(c), Inverse Pole Figures (IPFs) in the different grain orientations in the three fusion zones. Fig. 5(d)–(f) displays the grain misorientation distribution in the fusion zone of three investigated steels. The misorientation is found to be smallest in the fusion zone of Q&P980 steels, which could attribute the ductility during tensile process. A slight increase of grain misorientation is observed in the fusion zone of DP590 steels and largest grain misorientation is formed in the fusion zone of 22MnB5 steels. Large grain misorientation restricts the strain propagation, leading to the decrease of ductility. Variation of grain misorientations could have influence on the ductility of fusion zone.

3.2. STRAIN DISTRIBUTION

Using the DIC processing program, each captured image was analyzed to obtain the deformation and strain distribution during the de-formation. Fig. 6 illustrates the strain distribution of the specimens extracted from the fusion zone of Q&P980 steels, DP590 steels and 22MnB5 steels. The results show that the strain distribution is

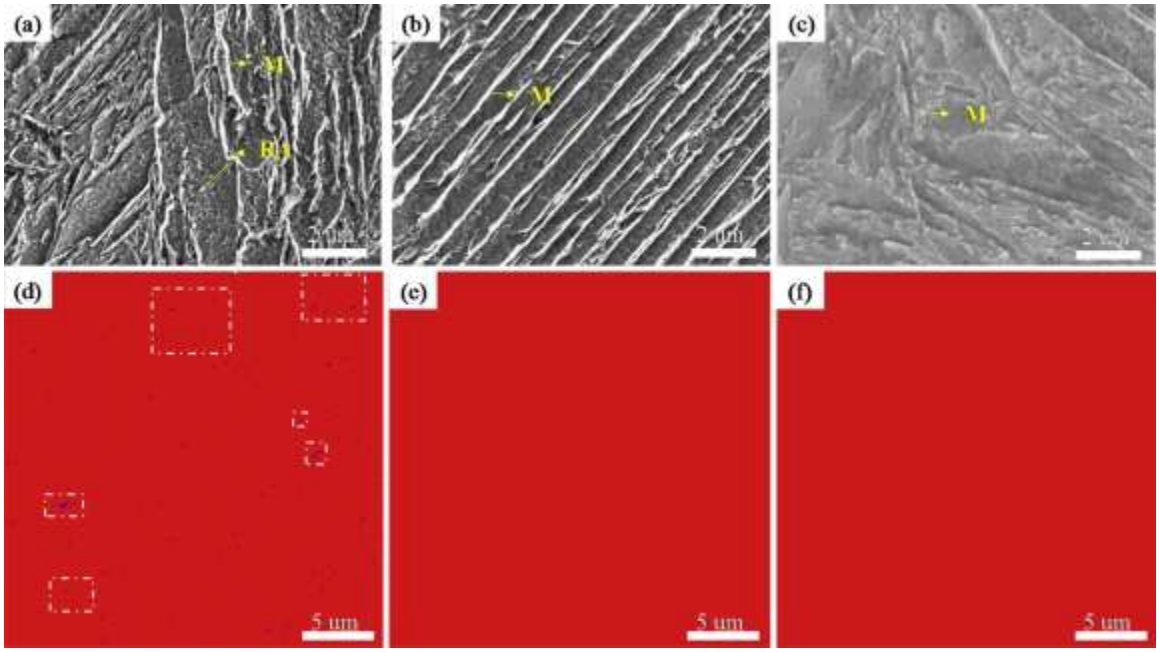

Fig. 4. Microstructure characterization of fusion zone before tensile test. (a), (b) and (c) depicts the microstructure of fusion zone in spot welds of Q&P980 steels, DP590 steels and 22MnB5 steels, respectively. M and RA is the abbriviation of martensite and retained austenite. (d), (e) and (f) depicts the phase distribution in the fusion zone of Q&P980 steels, DP590 steels and 22MnB5 steels. Red color and blue color in the mapping represent martensite phase and retained austenite phase, respectively (For interpretation of the references to colour in this figure legend, the reader is referred to the web version of this article).

inhomogeneous across the parallel region of small tensile specimen at the beginning of tensile tests (Fig. 6(a), (d), (g)), mainly due to the heterogeneous microstructure in the fusion zones. Variation in strength of intergranular and grain boundary contributes to the different strain in the two regions, resulting in the inhomogeneous strain distribution in the fusion zone at the beginning of tensile tests.

As tensile tests develops, the gradient in strain distribution of parallel region becomes shaper at maximum stress for all of the three steels as demonstrated in Fig. 6(b), (e) and (h). However, the strain concentration displays much more scatter of Q&P980 steels in com-parison with that of DP590 steels and 22MnB5 steels. This phenomenon could be explained by the different microstructure in the three fusion zones. The existence of retained austenite will accommodate the dy-namic strain during tensile tests. In the case of DP590 steels and

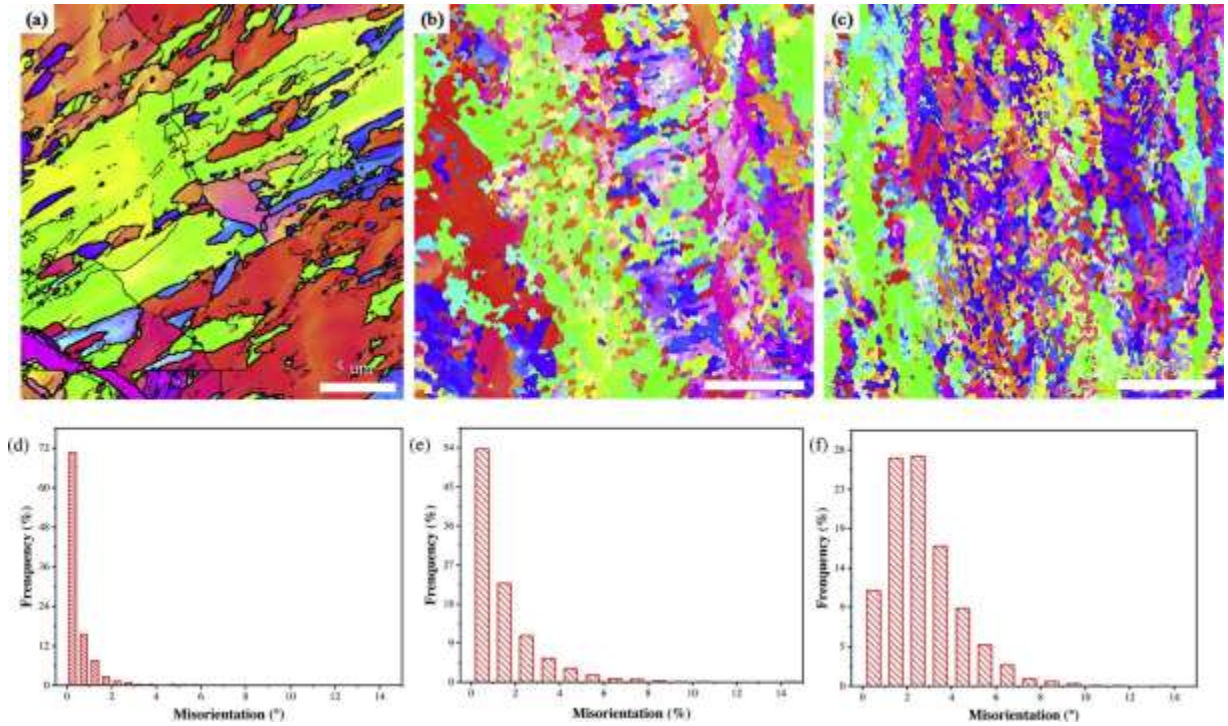

Fig. 5. Misorientations of the three fusion zones. (a), (b) and (c) presents the grain misorientations in the fusion zone of Q&P980 steels, DP590 steels and 22MnB5 steels.

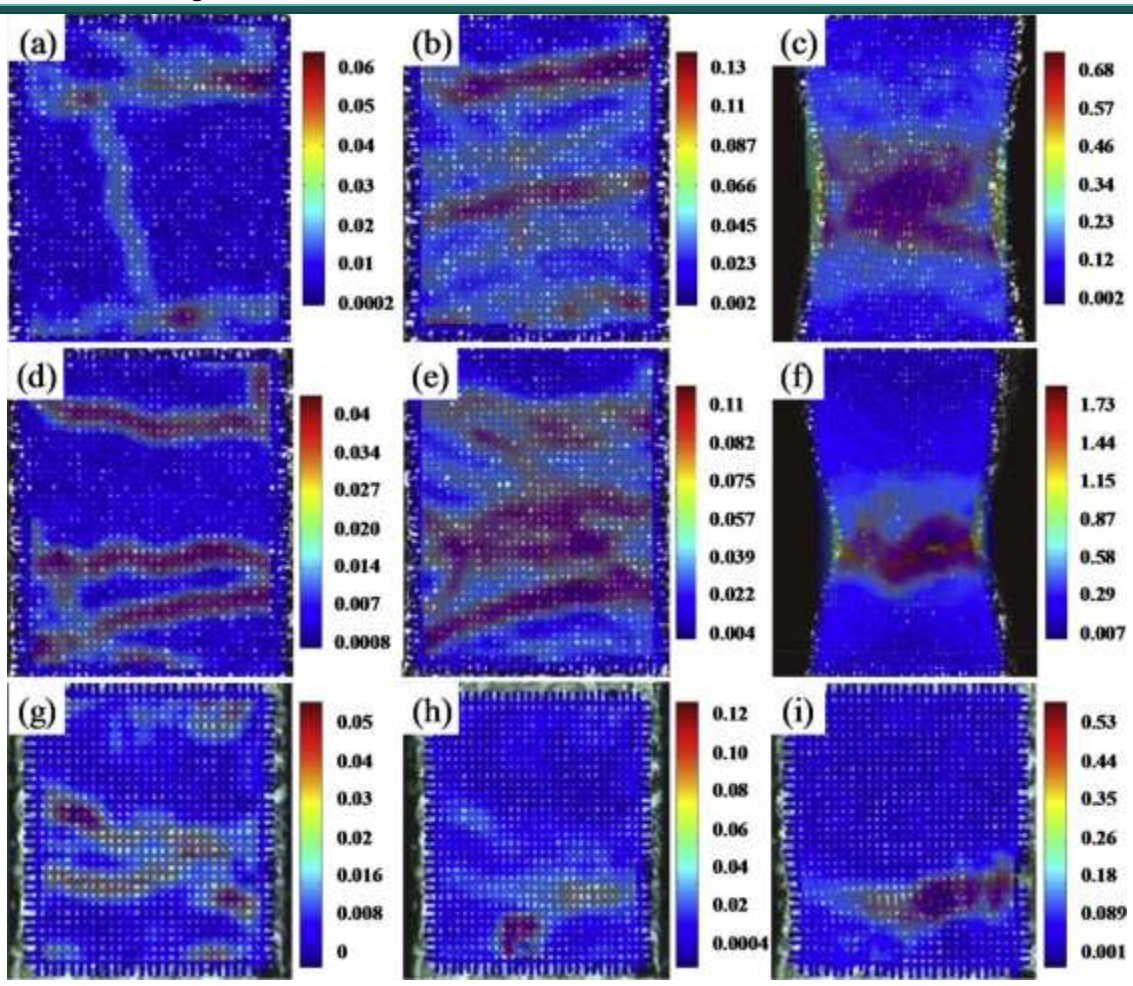

Fig. 6. Strain distribution in the fusion zone of three investigated steels. (a), (b) and (c) describes the strain distribution at 1%, maximum stress and fracture in fusion zone of Q&P980 steels. (d), (e) and (f) depicts the strain distribution at global elongation of 1%, maximum stress and fracture in the small tensile specimen extracted from the spot welds of DP590 steels. (g), (h) and (i) demonstrates the strain distribution of fusion zone corresponding to 1%, maximum stress and at fracture in the spot welds of 22MnB5 steels.

22MnB5 steels, high local misorientation in the martensite limits the strain accommodating capacity, which gives rise to the stress con-centration at moment of maximum stress.

At the failure, the deformation of specimens is localized at the necking area leading to a sharply increase of maximum strain at frac-ture for the condition of Q&P980 steels (Fig. 6(c)) and DP590 steels (Fig. 6(f)). However, it is not observed at the failure of fusion zone in 22MnB5 steels. This phenomenon is ascribed to the various failure modes in the three samples. Ductile failure forms in the fusion zone of Q &P980 steels and DP590 steels, and brittle failure reveals for 22MnB5 steels. The fracture beha vior of fusion zone in the three investigated steels will be investigated by the microstructure characterization of fractured specimen in the following parts.

Fig. 7 represents the strain distribution along the centerline of the parallel region in the fusion zone three investigated steels at three stages during deformation, which is the stage of 1%, at the moment of maximum stress and at failure. In the both cases of DP590 steels and 22MnB5 steels as depicted in Fig. 7(b) and Fig. 7(c), the strain gradient in the fusion zone is dramatic at failure and the strain concentration locates at the same position as the moment of maximum stress. How-ever, as shown in Fig. 7(a), the strain concentrates in four regions at the moment of maximum stress and the fusion zone fractures at one of the areas for the fusion zone in spot welds of Q&P980 steels. These results could confirm that the microstructure with retained austenite accom-modates the dynamic strain in the fusion zone of Q&P980 steels during the tensile tests.

3.3. FRACTURED BEHAVIOR

The microstructures of fusion zone after tensile test are illustrated in Fig. 8 for spot welds of Q&P980 steels, DP590 steels and 22MnB5 steels. In the Q&P980 steels shown in Fig. 8(a), it can be figured out that the martensite is extensively deformed and

elongated along the tensile di-rection. In the case of DP590 steels in Fig. 8(b), the deformation sub-structure in the martensite is not well developed compared to that of fusion zone in Q&P980 steels after tensile test. However, the de-formation of martensite in 22MnB5 steels (Fig. 8(c)) is not obvious. Thus, the strain localization and plastic deformation of martensite is more intense in the fusion zone of Q&P980 steels, which is mainly at-tributed to the microstructure with the formation with retained auste-nite. Retained austenite with small grain misorientations in the fusion zone will enhance the dynamic strain partitioning process during ten-sile test and enable a larger plastic deformation capacity.

The microstructure examination of fractured interface was con-ducted on the small tensile specimen extracted from the three in-vestigated steels and the results are revealed in Fig. 9. As illustrated in Fig. 9(a), dimples are observed in the fractured interface of fusion zone of Q&P980 steels, indicating the substantial plastic deformation in the zone during tensile tests. Trans granular ductile failure occurs after the alignment of micro-cavities caused by the imperfections and residual

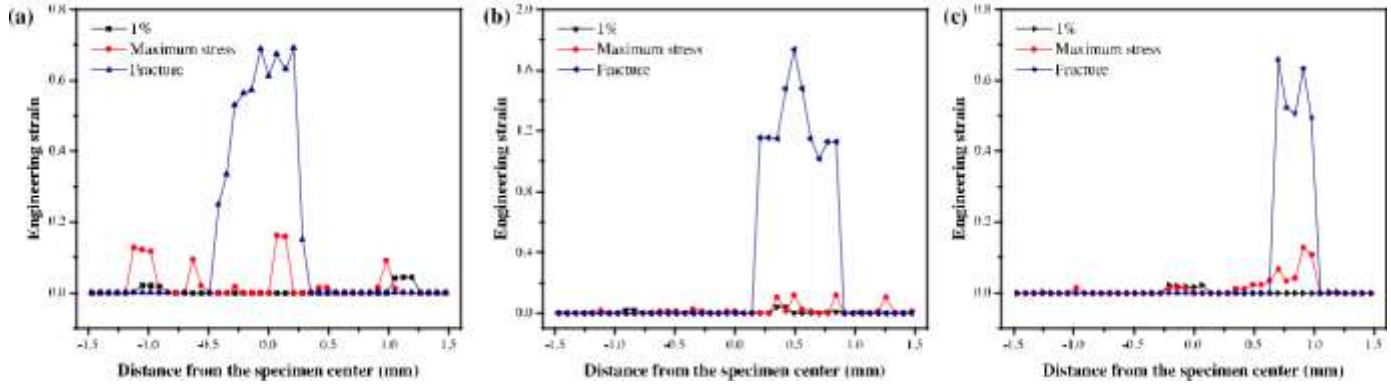

Fig. 7. Strain distributions along the center of small tensile specimen at various global elongations. (a), (b) and (c) represents the strain curves in the fusion zone of Q &P980 steels, DP590 steels and 22MnB5 steels, respectively.

Fig. 8. Microstructure characterization of fusion zone in the small tensile specimen after tensile test. (a), (b) and (c) depicts the microstructure of fusion zone in spot welds of Q&P980 steels, DP590 steels and 22MnB5 steels, respectively.

stress in the fusion zone. As for DP590 steels shown in Fig. 9(b), shallow simples are displayed in the zone, suggesting the failure behavior of cleavage fractures. This result indicates the insufficient plastic de-formation with a comparison to the fusion zone of Q&P980 steels. In the case of 22MnB5 steels as depicted in Fig. 9(c), the dimples are not obvious and the fracture mode is determined as brittle failure. This phenomenon could be explained by the microstructure evolution during tensile test. The martensite deformation during tensile tests (as illu-strated in Fig. 8(a) and (b)), attribute to the plastic deformation during tensile tests, leading to the formation of ductile failure in the fusion zone of Q&P980 steels and DP590 steels.

3.4. CONSTITUTIVE RELATIONSHIP

The true stress-strain curves of the fusion zones in the spot welds of Q&P980 steels, DP590 steels and 22MnB5 steels were obtained adopting designed small tensile specimen. Five replicates were con-ducted for each test and the results are shown in Fig. 10. Based on the results of five replicates as shown in Fig. 10(a)–(c), good repeatability is achieved in the stress-strain curves of fusion zone in the spot welds of Q &P980 steels, DP590 steels and 22MnB5 steels. In addition, the stress increases rapidly for the three steels, suggesting that the fusion zones exhibit a high yield strength. It is attributed to the high word-hardening rate at the beginning of the deformation caused by the multiplication of dislocation [25].

To make a comparison on the constitutive relationship in the fusion zones of Q&P980 steels, DP590 steels and 22MnB5 steels, the average of five stress-strain curves is extracted from the five replicates and the results are shown in Fig. 10(d). As can been seen, there are large difference between the fusion zones of different steels in both ultimate tensile strength and elongation. The ultimate tensile strength is close to 1700 MPa for the fusion zone of Q&P980 steels, whereas the fusion zones of DP590 steels and 22MnB5 steels both show similar ultimate tensile strength of 1100 MPa. Microstructure with retained austenite in the fusion zone of Q&P980 steels attributes to the improvement of ultimate tensile strength in the zone. Block martensite in the fusion zone of

22MnB5 restricts the strength improvement in the fusion zone, leading to the similar ultimate tensile strength with the fusion zone of DP600 steels.

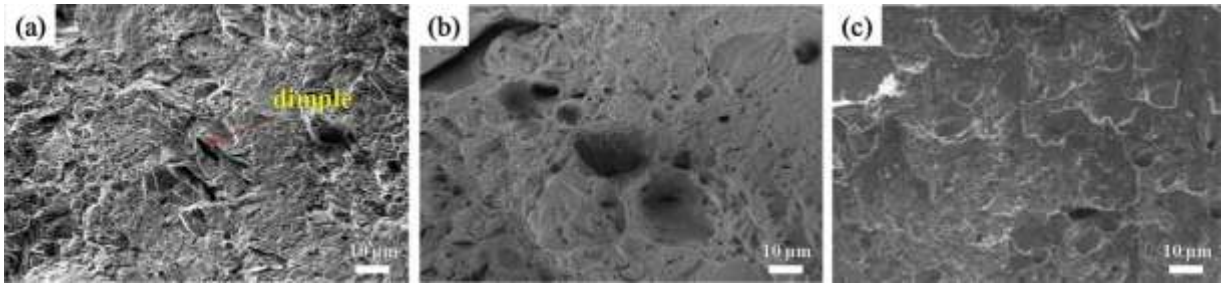

In the case of fracture strain, the three fusion zones show the same stress-strain response before reaching the yield stress. However, variation in the strains is observed in the fusion zone with the increase of

Fig. 9. Microstructure characterization of fracture interface in the small tensile specimen after tensile test. (a), (b) and (c) depicts the examination of fractured specimens of Q&P980 steels, DP590 steels and 22MnB5 steels, respectively.

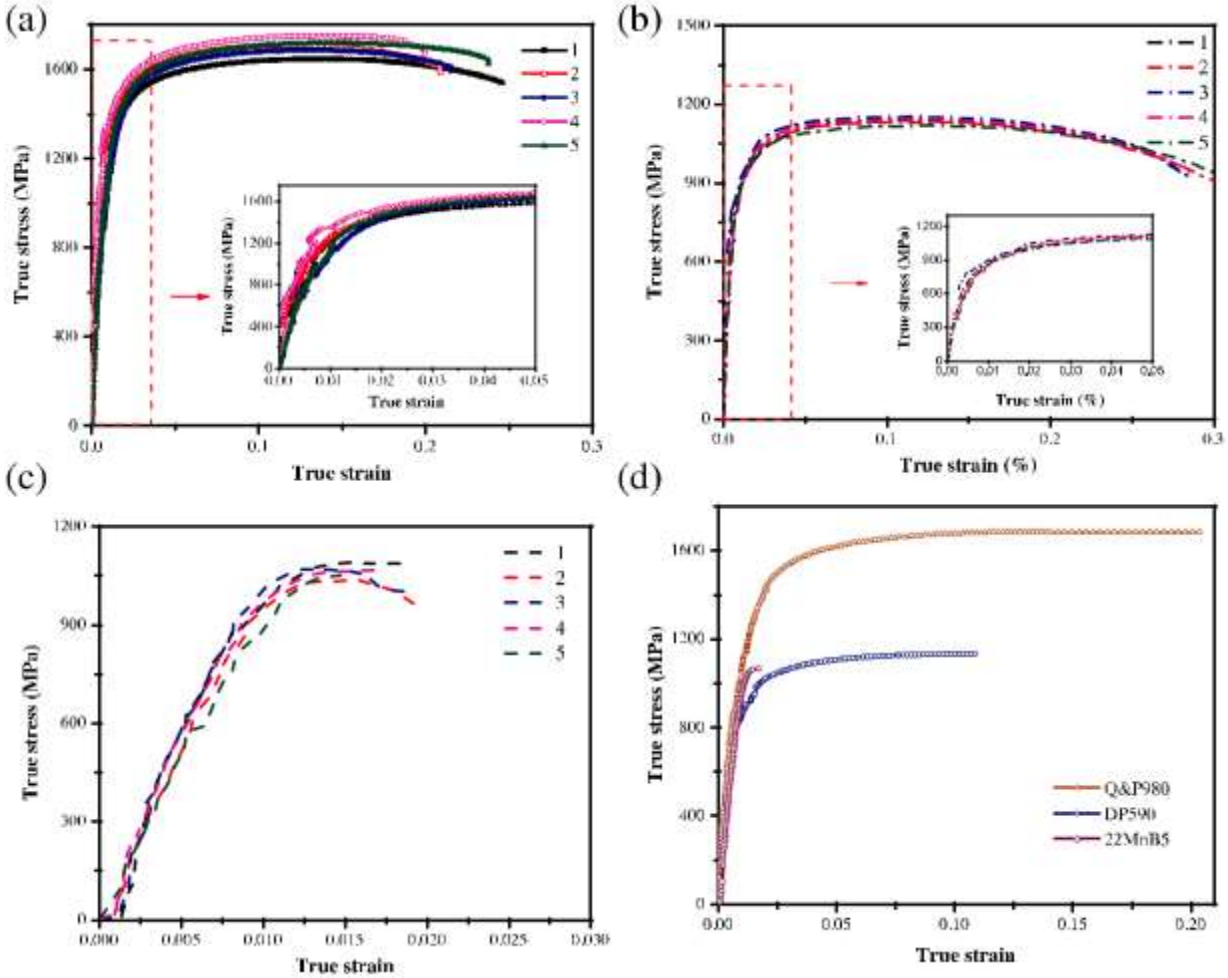

Fig. 10. Constitutive relationship of fusion zone extracted from small tensile specimen assisted with DIC technique. (a), (b) and (c) describes the true stress-strain curves of fusion zone in spot welds of Q&P980 steels, DP590 steels and 22MnB5 steels, respectively. (d) depicts the comparison of the three investigated steels before fracture in terms of true stress-strain curves.

strain. Later in the deformation process, the stress increase enables server deformation of the fusion zone in 22MnB5 steels. The strain localization is more rapid in the 22MnB5 steels leading to high strain hardening and early fracture in the zone. In the case of fusion zone in Q &P980 steels, a relatively low strain hardening is revealed and the fracture strain reaches more than 0.2, which is about twice than that of DP590 steels.

These results indicate that the fusion zone of Q&P980 steels exhibits superior strength and ductility than that of DP590 steels and 22MnB5 steels. These results could be explained by the following reasons. Firstly, the unevenly distributed carbon element in the fusion zone. Microstructure with high carbon content attribute to the improvement of strength in the fusion zone. Low carbon

microstructure accom-modates the dynamic strain during tensile tests, resulting in the large fracture strain of fusion zone. Second, the grain refinement in the martensite. Compared to the other two steels, the film-type austenite in the base metal of Q&P980 steels delays the austenite to martensite transformation during RSW process, resulting in the finer martensite in the fusion zone. Third, the effect of alloy element. Microstructure in the fusion zone with lower amount of C and higher amount of Mn attribute to the improvement of strength and ductility [24]. Last but not the least, the formation of retained austenite. The existence of retained austenite could accommodate the dynamic strain during tensile process, leading to the improvement of ductility in the fusion zone. All of these drives the superior mechanical properties in the fusion zone of Q&P980 steels when compared with that of DP590 steels and 22MnB5 steels.

Last but not the least, the formation of retained austenite. The existence of retaiend austenite could accommadate the dynamic strain during tensile process, leading to the improvement of ductlity in the fusion zone.

To make a further investigation on the constitutive relationship of fusion zone, the comparison with base metal is conducted. Fig. 11 de-scribes the representative ultimate tensile strength of the base metal and fusion zone in spot welds of Q&P980 steels, DP590 steels and 22MnB5 steels. Both ultimate tensile strengths increase in the fusion zone of Q&P980 steels and DP590 steels, which is about 38% and 60%, respectively. On the contrast, the 22MnB5 steels shows a lower ultimate tensile strength in the fusion zone. Similar results are observed in terms of strength improvement during the welding process, which is determined as the ratio of the ultimate tensile strength of the fusion zone to the corresponding base metal. Both Q&P980 and DP590 joints reaches as high as about 140% and 160%, respectively and only 70% is achieved in the joints of 22MnB5 steels. These results are largely attributed to the microstructure of the base metal in the three studies steels. Ferrite matrix in the base metal transforms to austenite and subsequently martensite on rapid cooling during RSW process, which will improve the fusion zone strength leading to high ratio of fusion zone strength and base metal strength in spot welds.

Fig. 12 depicts the fracture strain comparison results between fusion zone and base metal in spot welds of Q&P980 steels, DP590 steels and 22MnB5 steels. All the fracture strains after welding are observed smaller than those of the base metal. In the case of Q&P980 steels and

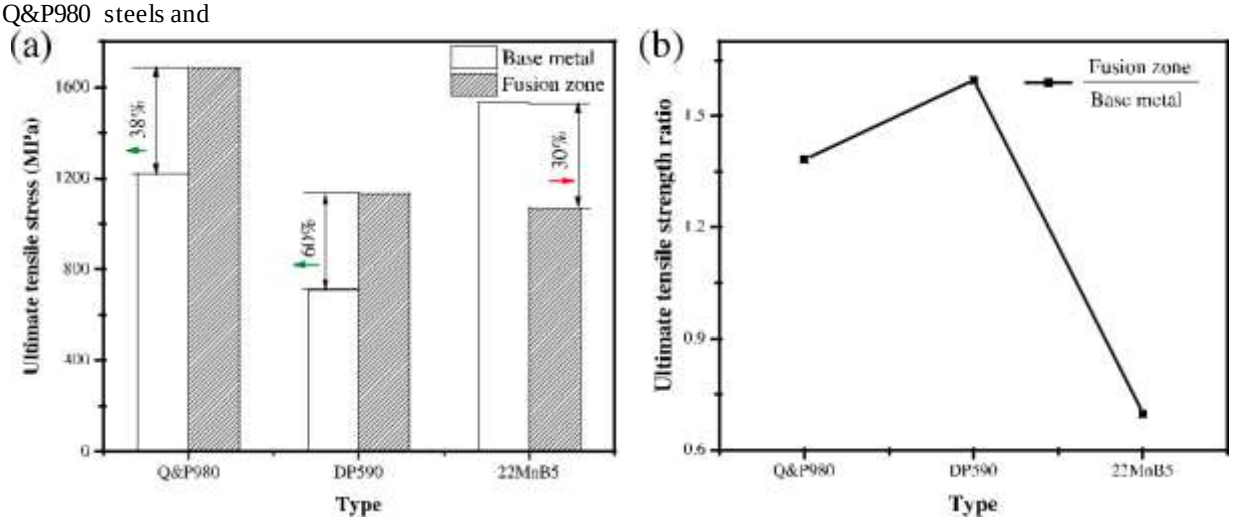

Fig. 11. Strength comparison in the spot welds of the three investigated steels. (a) is the ultimate tensile strength of the fusion zone and base metal. (b) describes the ratio of fusion zone strength and base metal strength in the spot welds.

22MnB5 steels, the existence of ferrite phase attributes to the higher fractures strain in the in the base metal. The fracture strain was higher for the ductile ferrite phase compared to the brittle martensite phase [12]. In the case of 22MnB5 steels, the block martenstie in the fusion zone restricts the plastict deformation, resulting in the decrease of fracture strain.

On the condition of fracture strain ratio, the spot welds of Q&P980 steels is approximately 1.0, indicating that the fracture strain in the fusion zone of Q&P980 steels is much closer to that of the base metal and a little decrease occurs during the welding process. This result is due to the formation of retained austenite in the microstructure of fu-sion zone. The microstructure with retained austenite and small grain orientations accommodates the dynamic strain during tensile test, re-sulting in the improvement of fracture strain in the fusion zone.

4. DISCUSSION

4.1. EFFECT OF CARBON EQUIVALENT

The aforementioned variation in the mechanical properties of fusion zone extracted from Q&P980, DP590 and 22MnB5 is largely attributed to the change in carbon equivalent, which is because the microstructure evolution is sensitively to the carbon equivalent in the material. The carbon equivalent is calculated by the equation for steels [26]:

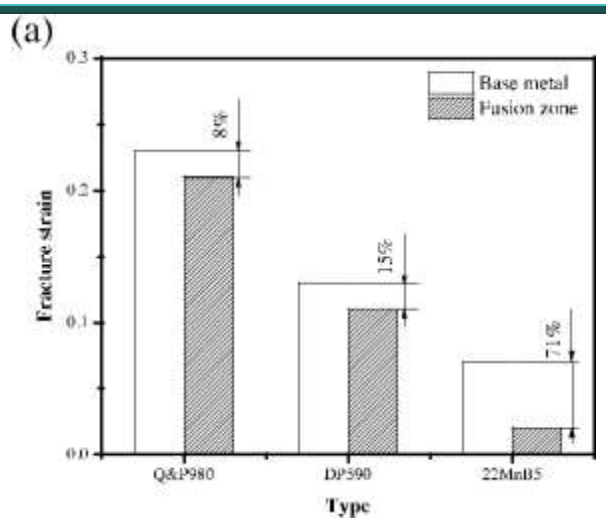

The carbon equivalent increases in the order of the 22MnB5, Q& P980 and DP590 steels (0.44, 0.57 and 0.59 respectively). The fusion zone of Q&P980 steel has the highest ultimate tensile strength and fracture strain among the three steels as shown in Fig. 10 (d). In the fusion zone containing retained austenite and lath martensite, the tensile strength is relatively higher while the fracture stain is maintained good. In order to obtain fusion zone having excellent combination of strength and ductility of A HSS, it is needed to develop the for-mation of martensite mixed with retained austenite. It is desirable to use approximate carbon equivalent and welding conditions for variously mixed martensite, such as in the fusion zone of Q&P980 steel. These results are useful for the development of AHSSs that could be applied to the structure component in the automotive industry re-quiring good combination of strength and ductility. In the future, sys-tematic investigations are required on microstructure evolution in the fusion zone to improve the mechanical properties of spot welds via alloying compositions optimizations.

4.2. EFFECT OF BASE METAL

In the current study, the primary distinction between the three in-vestigated steels is the microstructure difference in the base metal caused by various manufacturing process.

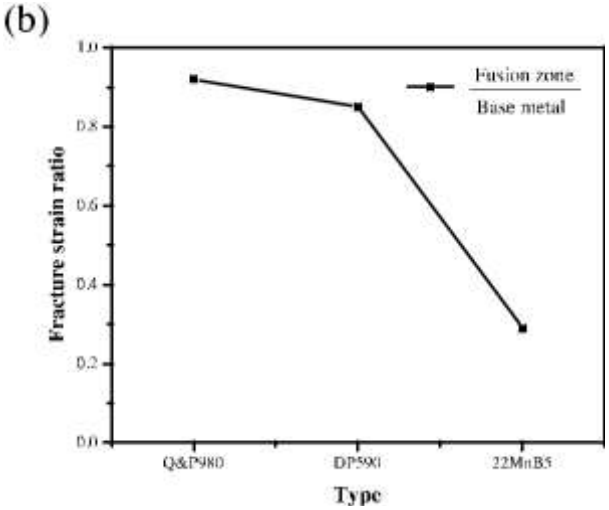

Fig. 12. Fracture strain comparison in the spot welds of the three investigated steels of Q&P980 steels, DP590 steels and 22MnB5 steels. (a) is the fracture strain of the fusion zone and base metal. (b) describes the ratio of fracture strain between fusion zone and base metal.

The mechanical properties of fusion zone are largely attributed to the martensite transformation during RSW process. In this paper, the fusion zone of Q&P980 steel has a good combination of tensile strength and ductility due to the existence o f retained austenite. Its formation is largely attributed to the quenching and partitioning process in the base metal of Q&P980 steel. Speer [27] defined the heat treatment process that could have retained austenite and tailored amounts of martensite. In the quenching process, austenite was quenched below the martensite transformation temperature to obtain martensite-austenite structure, and subsequently treated at the higher partitioning temperature. During the partitioning process, carbon diffused from martensite to retained

austenite to enhance its stability. It is suggested that stable retained austenite could attribute to the formation of martensite mixed of retained austenite in the fusion zone, leading to the improvement of tensile strength and ductility.

4.3. VIABILITY OF THE DIC METHOD

The DIC method proved to be a useful tool for extracting the con-stitutive relationship of the fusion zone in spot welds, where the small size of the fusion zone prohibits more conventional specimen extraction methods. The DIC results provide a quantitative assessment of the constitutive relationship in the fusion zone of spot welds. The true stress-strain curves provided by DIC analysis, such as shown in Fig. 10, provide potential input for high fidelity finite-element methods to predict the failure modes of spot welds. Furthermore, the strain distributions such as shown in Figs. 6 and 7 could provide a basis for validating the strain fields predicted by numerical models. In the cur-rent study, for the small tensile specimen extracted from the fusion zone, the cross-sectional plane at the center of parallel region is selected to be the joined interface of the two steel sheet. [18] has revealed that the stress-strain relation in the necking region of a thin sheet deviated subtle difference from that of uniaxial tension, despite the occurrence of heterogeneous strain distribution.

The DIC technique could prove useful in assessing the constitutive relationship of fusion zones. Some estimates are made as to the strengthening effect of grain size and phase transformation. However, a more thorough approach including advanced characterization of fusion zone microstructure could provide important understanding of the microstructure-property relations in the fusion zone of AHSSs.

5. CONCLUSIONS

This paper investigates and analyzes the constitutive relationship of fusion zone in advance high strength steels of Q&P980 steel, DP590 steels and 22MnB5 steels. The principle conclusions are summarized as follows:

(1) A new small tensile specimen was proposed in this paper to chacterize the constitutive relationship of fusion zone by using typical univeral testing machines.

(2) The fusion zones of DP590 steels and 22MnB5 steels both show similar ultimate tensile strength of 1100 MPa due to the formation of martensite. For the fusion zone of Q&P980 steels, the ultimate tensile strength is close to 1700 MPa because the existence of re-tained austenite.

(3) Heterogeneous microstructure with smaller grain misorientations leads to the more scatter strain distribution in the fusion zone of Q& P980 steels, resulting in larger fracture strain in a comparison with that of DP590 steels and 22MnB5 steels under the tensile test conditions.

(4) For the ratio of fusion zone strength and base metal strength, both spot welds of Q&P980 steels and DP590 steels reach as hig h as about 140% and 160%, respectively and only 70% is achieved in the spot welds of 22MnB5 steels. The fracture strain in the fusion

6. REFERENCES

[1] Pouranvari M, Marashi SPH. Critical review of automotive steels spot welding: process, structure and properties. Sci Technol Weld Join 2013;18:361–403.

[2] Shamanian M, Esmailzadeh M, Razmpoosh MH. The microstructural evolution and mechanical properties of resistance spot welded Fe-31Mn-3Al-3Si TWIP steel. Mater Eng 2015;67:571–6.

[3] Chabok A, van der Aa E, De Hosson JTM, Pei YT. Mechanical behavior and failure mechanism of resistance spot welded DP1000 dual phase steel. Mater Des 2017;124:171–82.

[4] Vargas VH, Mejía I, Baltazar-Hernández VH, Maldonado C. Characterization of re-sistance spot welded transformation induced plasticity (TRIP) steels with different silicon and carbon contents. J Manuf Process 2018;32:307–17.

[5] Zhang Y, Zhang X, Guo J, Manladan SM, Luo Z, Li Y. Effects of local stiffness on the spot joints mechanical properties: comparative study between resistance spot welding and resistance spot clinching joints. J Manuf Process 2019;39:93–101.

[6] Spena PR, De Maddis M, Lombardi F. Mechanical strength and fracture of resistance spot welded advanced high strength steels. Procedia Eng 2015;109:450–6.

[7] Dancette S, Fabregue D, Estevez R, Massardier V, Dupuy T, Bouzekri M. A finite element model for the prediction of Advanced High Strength Steel spot welds fracture. Eng Fract Mech 2012;87:48–61.

[8] Nikoosohbat F, Kheirandish S, Goodarzi M, Pouranvari M, Marashi SPH. Microstructure and failure behaviour of resistance spot welded DP980 dual phase steel. Mater Sci Technol 2013;26:738–44.

[9] Chung K, Noh W, Yang X, Han HN, Lee M-G. Practical failure analysis of resistance spot welded advanced high-strength steel sheets. Int J Plast 2017;94:122–47.

[10] Wang RJ, Shang DG. Low-cycle fatigue life prediction of spot welds based on hardness distribution and finite element analysis. Int J Fatigue 2009;31:508–14.

[11] Wang J, Xia Y, Zhou Q, Zhang J. Simulation of spot weld pullout by modeling failure around nugget. SAE Technical Papers. 2006.
[12] Eller TK, Greve L, Andres MT, Medricky M, Hatscher A, Meinders VT, et al. Plasticity and fracture modeling of quench-hardenable boron steel with tailored properties. J Mater Process Technol 2014;214:1211–27.
[13] Kang J, McDermid JR, Bruhis M. Determination of the constitutive behaviour of AA6022-T4 aluminium alloy spot welds at large strains. Mater Sci Eng A 2013;567:95–100.
[14] Lee H, Kim C, Song J. An evaluation of global and local tensile properties of friction-stir welded DP980 dual-phase steel joints using a digital image correlation method. Materials 2015;8:8424–36.
[15] Gronostajski Z, Niechajowicz A, Kuziak R, Krawczyk J, Polak S. The effect of the strain rate on the stress-strain curve and microstructure of AHSS. J Mater Process Technol 2017;242:246–59.
[16] Chen J, Feng Z. Strain and distortion monitoring during arc welding by 3D digital image correlation. Sci Technol Weld Join 2018;23:536–42.
[17] Chen J, Tatman J, Chen Z, Feng Z, Frederick G. Proactive in-situ welding stress control for laser repair welding of irradiated austenitic materials. 2017.
[18] Tong W, Tao H, Jiang X, Zhang N, Marya MP, Hector Jr LG, et al. Deformation and fracture of miniature tensile bars with resistance-spot-weld microstructures. Metall Mater Trans A: Phys Metall Mater Sci 2005;36:2651–69.
[19] Park N, Park M, Kwon J, Huh H. Material properties of the nugget zone in resistance spot-welded DP980 steel joint at various strain rates. Sci Technol Weld Join 2017;23:7–12.
[20] Liu H, Shen Y, Yang S, Zheng P, Zhang L. A comprehensive solution to miniaturized tensile testing: specimen geometry optimization and extraction of constitutive be-haviors using inverse FEM procedure. Fusion Eng Des 2017;121:188–97.
[21] Xu ZT, Peng LF, Lai XM, Fu MW. Geometry and grain size effects on the forming limit of sheet metals in micro-scaled plastic deformation. Mater Sci Eng A 2014;611:345–53.
[22] Pan B, Asundi A, Xie H, Gao J. Digital image correlation using iterative least squares and pointwise least squares for displacement field and strain field measurements. Opt Lasers Eng 2009;47:865–74.
[23] Lava P, Coppieters S, Wang Y, Van Houtte P, Debruyne D. Error estimation in measuring strain fields with DIC on planar sheet metal specimens with a non-per-pendicular camera alignment. Opt Lasers Eng 2011;49:57–65.
[24] Stormvinter A, Miyamoto G, Furuhara T, Hedström P, Borgenstam A. Effect of carbon content on variant pairing of martensite in Fe–C alloys. Acta Mater 2012;60:7265–74.
[25] Lin YC, Li K-K, Li H-B, Chen J, Chen X-M, Wen D-X. New constitutive model for high-temperature deformation behavior of inconel 718 superalloy. Mater Des
[26] Sung HK, Shin SY, Hwang B, Lee CG, Kim NJ, Lee S. Effects of carbon equivalent and cooling rate on tensile and Charpy impact properties of high-strength bainitic steels. Mater Sci Eng A 2011;530:530–8.
[27] Speer J, Matlock DK, De Cooman BC, Schroth JG. Carbon partitioning into austenite after martensite transformation. Acta Mater 2003;51:2611–22.